Controllable step motors and rectifiers of magnetic flux quanta using periodic arrays of asymmetric pinning defects

B. Y. Zhu,[1] F. Marchesoni,[1,2] V. V. Moshchalkov,[3] and Franco Nori[1,4,*]

[1]*Frontier Research System, The Institute of Physical and Chemical Research (RIKEN), Wako-shi, Saitama 351-0198, Japan*
[2]*Istituto Nazionale di Fisica della Materia, Universitá di Camerino, I-62032 Camerino, Italy*
[3]*Laboratorium voor Vaste-Stoffysica en Magnetisme, Katholieke Universiteit Leuven, B-3001 Leuven, Belgium*
[4]*Center for Theoretical Physics, Physics Department, Center for the Study of Complex Systems, The University of Michigan, Ann Arbor, Michigan 48109-1120, USA*

We study the transport of vortices in superconductors with regular arrays of asymmetric pinning wells when applying an alternating electrical current. The asymmetric traps are modelled by the superposition of two interpenetrating square lattices of weak and strong pinning centers with separation smaller than the lattice constant. We show that this system can induce a net rectifying or diode effect for the vortex motion, including collective step-motor-type dynamics, where many vortices move forward a controlled and exact number of pin-lattice spacings at each cycle of the ac driving force. This system exhibits a remarkable net dc response with striking sawtooth-type oscillations. The net dc voltage response V_{dc} of the ac-driven vortices versus both the half period P and the amplitude F_L of the "square wave" ac drive has been detailed in the present work. The influence of the equilibrium thermal noise, the shift between the two pinning sublattices, the degree of translational and orientational disorder, and the size of the simulation system on the V_{dc} response of the vortex motion at ac drive has also been addressed. Devil staircase and Arnold's tongue structures are revealed. We also analytically derive all the key features of our numerical results. This system provides a very controllable stepmotor for the control of collective motion. Our results apply *mutatis mutandis* to arrays of Josephson junctions, colloidal systems with optical traps, Wigner crystals, and any system with repelling movable objects that can be pinned by a lattice of traps.

I. INTRODUCTION

Vortex dynamics in superconductors under the influence of an asymmetric periodic potential has attracted considerable interest in recent years. It can be used for designing flux pumps, rectifiers, or diodes, as well as for focusing and lensing flux quanta in designated target regions within a superconducting device.[1–6] The control of the motion of vortices using asymmetric pinning can be useful for applications in superconducting devices, including the removal of unwanted trapped flux in devices.[7] Recently, several groups[1–6,8–13] have made proposals for quite distinct ways of using potential energy ratchets in superconductors. Most of the earlier studies on ratchet-type systems focused on a *single* particle moving on a one-dimensional (1D) asymmetric potential, as opposed to motion in 2D potentials (e.g., Refs. 1 and 3–6) or in three-dimensions (as in Ref. 6). Also, other works[14–16] studying asymmetric pins considered dc-driven cases, which produce no vortex rectification.

A standard 1D potential-energy ratchet was used in Ref. 2 to move vortices inside superconducting samples using ac drives. 2D asymmetric channel walls were introduced in Ref. 1 and a graduated random pinning density was considered in Refs. 3 and 4, both rectifying the motion of interacting vortices. In such systems, the *collective interactions* among vortices are responsible for the dc transport of magnetic flux under the influence of an ac electrical current applied to the system. Simulations[3] and preliminary experiments[4] show that the ratchet effect of such pinning system works when the

number of vortices is larger than the number of pinning sites in the system. The system studied here rectifies the vortex motion for all values of the applied magnetic field, and not just above the first matching field. Indeed, it becomes a more effective vortex pump at and below the first matching field. Thus, it operates in a different magnetic field regime.

Further investigations of the effect of the asymmetry of the pinning array and the pinning sites themselves will help the design of more effective ways to control the motion of vortices in artificially nanostructured superconductors. One of the simplest ways to produce asymmetric pinning sites is to superimpose two interpenetrating arrays of weak and strong pinning sites.[15] This type of asymmetric geometry can be fabricated using electron-beam lithographic techniques.[17]

The results reported in this paper can be summarized as follows. Using molecular dynamics simulations, we investigated the stochastic rectification of ac-driven vortices due to the "ratchet effect" of asymmetric pinning traps. In contrast to Ref. 3, for an applied transverse ac electric current, we observe a net longitudinal transport of the vortices for *any* value of H/H_1, not just for $H/H_1>1$. Here H_1 is the field at which the total number of vortices N_v is equal to the number of pinning centers N_p. We have found that, for the two interpenetrating square pinning arrays with separation d, we can easily control of the collective motion of the vortices. We will also show how the net dc response, in the presence of an applied ac drive, varies as a function of (1) the distance d between the two pinning square sublattices, (2) the ratio of strong to weak pinning strength, (3) temperature, and (4) the
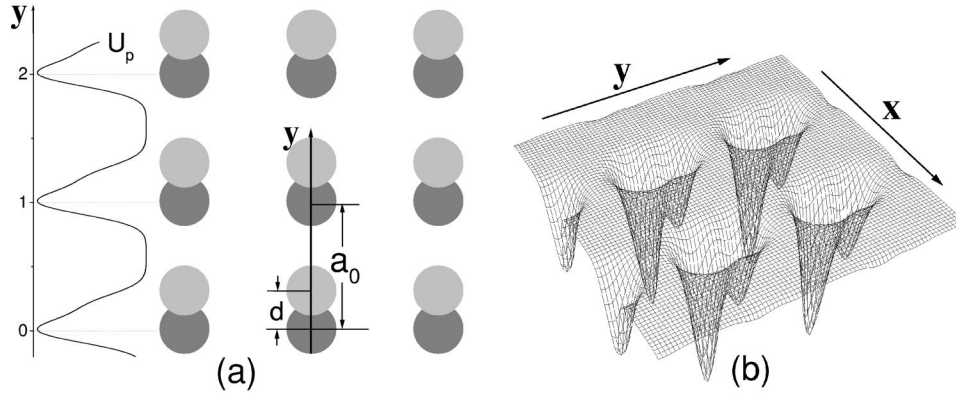
FIG. 1. (a) A 2D illustration of the two interpenetrating square lattices of pinning sites with $d=0.2a_0$. The period a_0 of both the strong pinning lattice (indicated here schematically by darker gray circles) and the weak pinning lattice (lighter gray circles) are the same. The shift between the strong and the weak pinning lattice along the y direction is denoted by d. Both pinning sites have the same size. The corresponding asymmetric pinning potential $U_p(y)$ is displayed for readers' convenience. (b) 3D illustration of the pinning potential of the interpenetrating lattices with $d=0.3a_0$.

frequency and amplitude of the drive. The effects of both translational and orientational disorder are also studied; in particular we detected a devil staircase structure in the system characteristics curve, which develops Arnold's tongues when disorder is systematically increased.

Moreover, we introduce an asymmetry factor for this class of devices proportional to the difference between the vortex depinning forces in opposite directions. Such an *asymmetry factor* is a crucial figure of merit characterizing the performance of this type of devices. We also analytically derive all the key features of our numerical results, including the remarkable net dc response with striking sawtooth-type oscillations.

II. MODEL

Figure 1(a) shows a schematic diagram of the top x-y view of a sample with interpenetrating arrays of weak and strong pinning sites. The strong and the weak pinning sites are placed on two square lattices with spacing a_0 and separated by a distance d in the y direction. Here, we choose $a_0 = 1$. Figure 1(b) shows a small portion of the potential energy landscape over which vortices move. All pinning centers are modeled by Gaussian potential wells[15,18] with a decay length R_p. The pinning force exerted by the kth pin of one sublattice on the ith vortex is

$$\mathbf{F}_p^\gamma(\mathbf{r}_i) = -F_{p0}^\gamma f_0 \frac{\mathbf{r}_i - \mathbf{R}_k^\gamma}{R_p} \exp\left(-\left|\frac{\mathbf{r}_i - \mathbf{R}_k^\gamma}{R_p}\right|^2\right), \quad (1)$$

where $\mathbf{r}_i$ represents the location of the ith vortex and $\mathbf{R}_k^\gamma$ is the location of the kth pin of the $\gamma = w$ ("weak") and the $\gamma = w$ ("strong") sublattice, respectively. The intensity of the individual pinning force is denoted by $F_{p0}^\gamma f_0$. The total pinning force acting on the vortex is obtained by adding up the single $\mathbf{F}_p^\gamma(\mathbf{r}_i)$ terms for both pinning sublattices.

In our simulation, forces (per unit length) are taken in units of $f_0 = \Phi_0^2/8\pi^2\lambda^3$, with Φ_0 the superconducting flux quantum and λ the superconducting penetration depth. Since

our pinning strengths F_{p0}^γ are unequal, the asymmetry of the lattice can be controlled by d. The driving force acting on the vortices is the Lorentz force $\mathbf{F}_L = \mathbf{J} \times \mathbf{\Phi}_0$, where $\mathbf{J}$ is an applied electric current. Here, an ac current is applied to the sample along the x direction in the x-y plane, so that the driving Lorentz force $\mathbf{F}_L$ is always parallel to the y axis, i.e., $F_L \equiv F_L^y$. The repulsive vortex-vortex interaction is modeled[19] by a logarithmic potential, $U_{vv} \sim -\ln(r/\lambda)$. Thus, the vortex-vortex interaction force is

$$\mathbf{F}_{vv}(\mathbf{r}_i) = F_{vv0} f_0 \sum_{j\neq i}^{N_v} \frac{\lambda \hat{\mathbf{r}}_{ij}}{|\mathbf{r}_i - \mathbf{r}_j|}, \quad (2)$$

where $\hat{\mathbf{r}}_{ij} = (\mathbf{r}_i - \mathbf{r}_j)/|\mathbf{r}_i - \mathbf{r}_j|$. The intensity of the intervortex interaction force is $F_{vv0} f_0$ and the cut-off length for such long-range force is set to $5a_0$. The overdamped equation of motion for vortex i is given by

$$\eta \mathbf{v}_i = \mathbf{F}_L + \mathbf{F}_{vv}(\mathbf{r}_i) + \mathbf{F}_p(\mathbf{r}_i) + \mathbf{F}_T, \quad (3)$$

where η is the viscosity coefficient, taken to be unity, and $\mathbf{F}_T$ represents the thermal contribution to the vortex motion. This is modeled[19] by

$$\mathbf{F}_T = F_{T_0} f_0 \sum_j \delta(t - t_j) \Gamma(t_j) \Theta(\omega - q_j), \quad (4)$$

where $F_{T_0} f_0$ stands for the intensity of the thermal fluctuations, which in turn is proportional to the square root of the temperature. The factor $\Gamma(t_j)$ is a random number chosen from a Gaussian distribution with zero mean and unit variance at each time $t_j = j\tau_0$; $\omega = \tau_0/\Delta$ is the probability that the noise term acts on a given vortex (τ_0 is the discrete time step and Δ is the mean time between two successive random noise pulses) and q_j is a random number uniformly distributed between 0 and 1. Finally, $\Theta(x)$ is the step function with $\Theta = 1$ for $x > 0$ and 0 for $x < 0$. Throughout the simulation work reported here, we chose $\tau_0 = 0.0067$ and $\omega = 0.9$.

The vortex equation of motion is solved by taking discrete time steps τ_0 in a 2D square sample containing two interpenetrating arrays of strong and weak pinning sites with periodic boundary conditions in both directions. The initial vortex positions are obtained by annealing: the sample is first exposed to high temperatures and then cooled down to zero temperature. Afterwards the sample is subjected to a square-wave alternating current along the x axis, producing a square-wave Lorentz driving force along the y axis with amplitude F_L and half-period P. The remaining simulation lengths and forces are kept constant: $R_p = 0.13a_0$, $\lambda = 2.6a_0$, $F_{vv0} = 0.1$, and $F_{p0}^s = 0.5$. Systematic simulation runs were carried out only for a square sample with size $10a_0 \times 10a_0$, (i.e., $N_p = 100$). We tested samples of different sizes and geometries, as well, coming to the conclusion that our results are insensitive to the sample size, provided that the density of vortices and pinning sites is kept constant.

A single trapped vortex can be extracted from an isolated composite pinning center by applying an external pull with amplitude larger than a characteristic *depinning force*, namely, $F_L > F_m$ when $\mathbf{F}_L \| \mathbf{y}$ and $F_L > F_M$ when $\mathbf{F}_L \| -\mathbf{y}$. For the pinning parameters adopted throughout the present work, one obtains numerically $F_m \simeq 0.236$ and $F_M \simeq 0.436$, respectively, for the weak and strong pin stopping forces. Notice that F_m and F_M deviate from the relevant pinning site strength in opposite way, that is $F_m > F_{p0}^w$ and $F_M < F_{p0}^w$.

III. VORTEX STEP MOTOR

To investigate the effect of asymmetric pinning on the vortex motion under the action of an ac drive, we set first the separation between the two pinning sublattices, $d = 0.2a_0$, and the relevant pinning strength ratio, $F_{p0}^s / F_{p0}^w = 2$, so as to maximize the asymmetry of the pinning potential $U_p(y)$ in Fig. 1(b).[15]

The key transport quantity to be studied in this work is

$$V_{dc} = \left\langle \frac{1}{N_v} \sum_i^{N_v} v_i \right\rangle_{ac} ,$$

where $\langle \ldots \rangle_{ac}$ denotes the stationary time-average over the forcing cycle.

Figure 2(a) shows V_{dc} versus P for different amplitudes F_L of the driving force. Each point plotted here was obtained by averaging vortex velocity (1) over 200 forcing periods, each with about 10^4 to 10^6 MD steps. Longer time averages taken over up to $10^3 P$ yielded a standard deviation for V_{dc} lower than 2%. Interestingly, on increasing the period of the driving force (from $P = 0$ up to $5000\tau_0$ with a small step $\Delta P = 10\tau_0$), sharp jumps in the rectified voltage $V_{dc}(P)$ curves appear mainly for drive amplitudes in the range (F_m, F_M).

The role of the drive half-period P in the rectification process is critical. When P is sufficiently small, the driven vortices cannot travel enough distance from one pinning site to another parallel to the driving force during a positive half-period P, i.e., when $\mathbf{F}_L \| \mathbf{y}$; the vortices will be then driven back to the original pinning sites during the subsequent negative half period with $\mathbf{F}_L \| -\mathbf{y}$, which results in a vanishingly
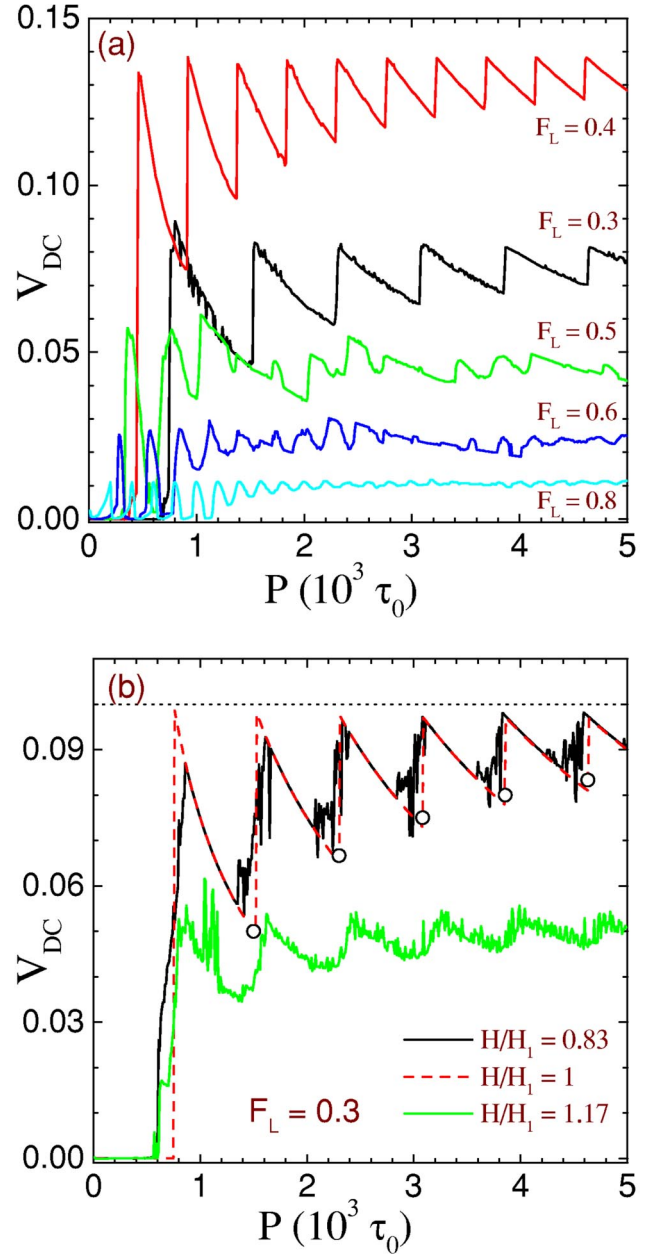

FIG. 2. (Color online) (a) Time-averaged net velocity V_{dc} vs the drive half-period P for different values of the forcing amplitude F_L and constant magnetic field $H/H_1 = 1.05$, in the absence of thermal noise. Notice the *nonmonotonic* behavior of $V_{dc}(P)$, with the largest V_{dc} values obtained for $F_L \sim 0.4$. (b) Curves $V_{dc}(P)$ for different ratios of vortices to pins in the sample (note that $N_v/N_p = H/H_1$) and fixed driving amplitude $F_L = 0.3$. The remaining simulation parameters are: $d = 0.2a_0$, $F_{p0}^s/F_{p0}^w = 2$, $\tau_0 = 0.0067$, and $F_{T_0} = 0$. In panel (b) the horizontal dotted line is V_M, Eq. (7), and the open circles represent $V_m(n)$, Eq. (8), for $n = 1$–5.

small dc response of the vortices. Note that in the absence of interactions with the pins and the surrounding vortices, the speed of an individual driven vortex would be F_L (as η was set to 1).

When the period of the driving force exceeds the threshold value $P_c \sim a_0/F_L$, for $F_m \lesssim F_L \lesssim F_M$ the vortices can

move a distance equal to or larger than the pinning lattice constant a_0 during a positive drive half-period; as a consequence, the vortices get blocked one or more pinning centers away from their starting location, in the y direction, as $\mathbf{F}_L$ reverses sign: the system acts as a vortex rectifier. Moreover, it may be regarded as a controllable collective "step motor" of flux quanta as many vortices move forward in unison.

The origin of the rectification effect can be explained as follows. Let us consider an individual vortex approaching a composite pinning unit, consisting of a strong and a weak pinning site, subject to a driving force with $F_m \lesssim F_L \lesssim F_M$. If the moving vortex enters the pinning center through the weak pinning site (negative half cycle), it gets stuck against the strong pin. In the opposite case (positive half cycle), after entering the pinning center the vortex is likely to climb over the less steep wall of the weak trap and thus exit the pinning center in the positive y direction. For arbitrarily large F_L values, depending on the direction of the drive, the vortices would then move either less or more distance in one half period than in the other one; this produces a rectified vortex transport in the positive direction.

To further clarify this mechanism in Fig. 3, we display the trajectories $y(t)$ of a *single* trapped vortex in the pinning potential $U_p(y)$; the corresponding velocities $v(t)$ and driving forces $F_L(t)$ are shown for the sake of a comparison. These trajectories have been obtained by simulating the time evolution of the collective vortex configuration at the first matching field, $H/H_1 = 1$, where there is one (trapped) vortex per pinning center and the vortex system moves rigidly in unison. Panels 3(a) and 3(b) contrast a locked versus a ratcheted vortex array at different values of P; the vortex stepwise motion with shifts a_0 and $2a_0$ per cycle, respectively, is illustrated in panels 3(b) and 3(c).

The striking sawtooth-type *oscillations* of $V_{dc}(P)$ for $P > P_c$ are a remarkable feature of this system. The very sharp peaks in V_{dc} locate the optimal periods for the ac driving force to produce maximum rectification. The distance $\tilde{P}$ between two oscillation peaks in each curve also depends on the drive amplitude F_L. As the optimal vortex displacement corresponding to two adjacent $V_{dc}(P)$ peaks is $\tilde{P} \times F_L \sim a_0$ [see Fig. 3(c)], the period $\tilde{P}$ of a $V_{dc}(P)$ oscillation nearly coincides with the threshold value P_c (see Sec. IX for a more detailed discussion).

The dependence of V_{dc} on the drive amplitude F_L is *nonmonotonic* as we proved by varying F_L from 0.3 to 0.8 in Fig. 2(a). If the drive amplitude is set below the rectification threshold (i.e., $F_L < F_m$), the trapped vortices cannot be depinned at all, which causes a highly suppressed dc response (a residual, mostly *negative*, contribution to V_{dc} may come from interstitial vortices moving away from the pin centers). On raising F_L above F_m, the collective vortex stepmotor mechanism sets on; vortices advance in the positive y direction increasingly larger multiples of the unit step a_0 per cycle. Eventually, as the driving force grows larger than the strong pin stopping force F_M, all vortices will move back and forth collectively, insensitive to the asymmetric pinning lattice [see Fig. 3(d)]; hence the very weak dc response at $F_L \simeq 0.8$ shown in Fig. 2(a). In conclusion the vortex net
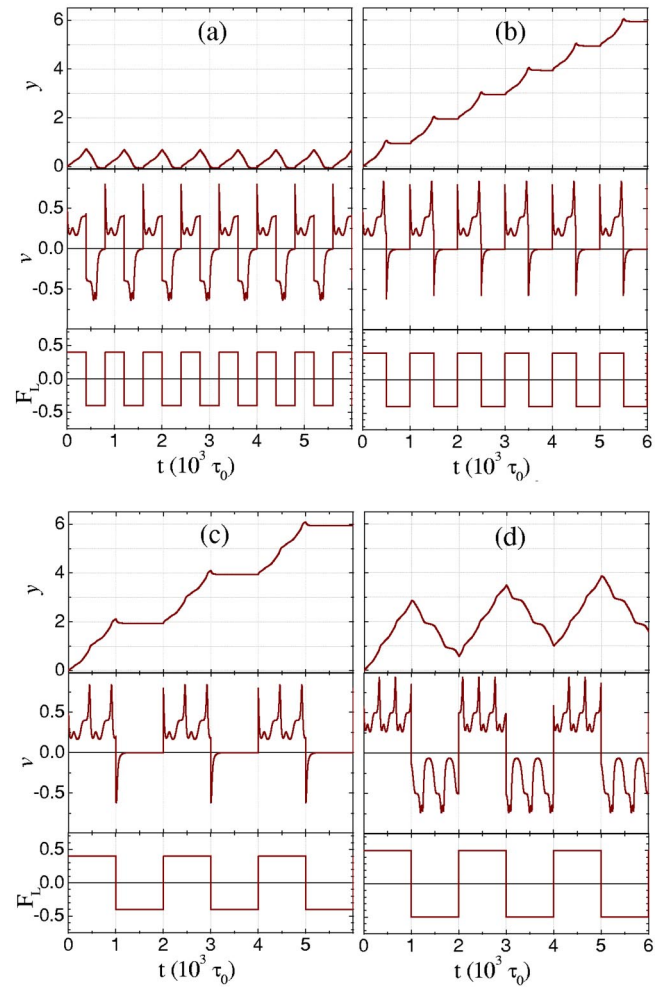

FIG. 3. (Color online) Vortex displacement y, velocity v and driving force as a function of time for different values of the half-period P and the amplitudes F_L of the ac drive at the first matching field $H/H_1 = 1$: (a) $P = 400\tau_0$, (b) $P = 500\tau_0$, (c) $P = 1000\tau_0$ at $F_L = 0.4$, and (d) $P = 1000\tau_0$ at $F_L = 0.5$. The remaining simulation parameters are $d = 0.2a_0$, $F_{p0}^s / F_{p0}^w = 2$, $F_{T_0} = 0$, and $\tau_0 = 0.0067$.

velocity attains necessarily a maximum for an appropriate value of the drive amplitude close to F_M.

In Fig. 2(b), we display the curves $V_{dc}(P)$ for different values of the applied magnetic field and a fixed drive amplitude $F_L = 0.3$. A nonzero net average vortex velocity is *always* observed, even when there are fewer vortices than pinning centers, that is $H < H_1$. This is a remarkable property, when compared with vortex rectification in samples with "gradual" random pinning.[3] There a nonzero dc response was obtained for $H/H_1 > 1$, only, whereas the present system can rectify the motion of any assembly of vortices for all values of H.

The threshold value P_c for the onset of vortex transport and the period $\tilde{P}$ of the $V_{dc}(P)$ oscillations in Fig. 2(b) are almost identical, irrespective of the applied magnetic field. The magnetic field density H/H_1, however, clearly impacts the magnitude of vortex response through the collective interaction among vortices. For $H/H_1 < 1$, (i.e., the number of vortices is smaller than the pins in the system), the rectifica-
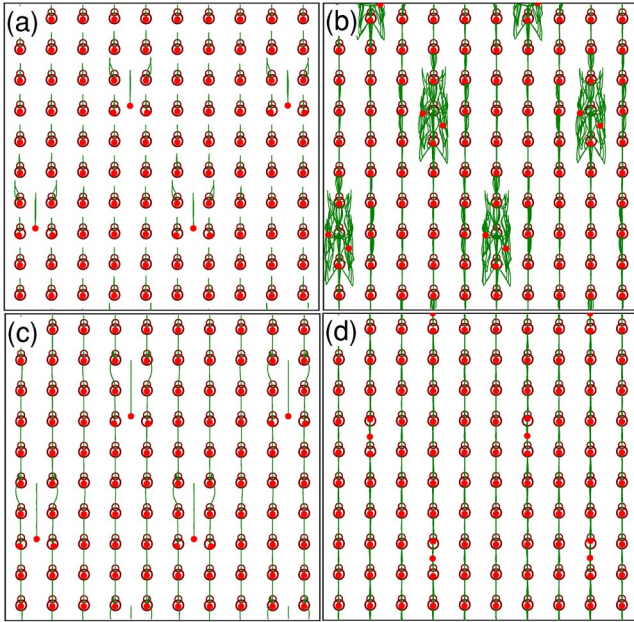
FIG. 4. (Color online) (a)–(d) Vortex trajectories at fixed amplitude $F_L = 0.3$ of the ac driving force for different half-periods $P = 600\tau_0$, $800\tau_0$, $1000\tau_0$, and $1600\tau_0$. Here $d = 0.2a_0$, $F_{p0}^s/F_{p0}^w = 2$, $F_{T_0} = 0$, $\tau_0 = 0.0067$, and $H/H_1 = 1.05$. The interstitial vortices shown in (a), (b), and (c), become incorporated in the lattice creating "solitonlike" discommensurations that propagate forward along the vertical columns.

tion effect is the most pronounced because the vortices can be trapped more efficiently by the pinning centers as they move back and forth during one drive period. On the contrary, for $H/H_1 > 1$ more and more interstitial vortices move back and forth rather freely, while the increased vortex density causes a stronger vortex-vortex repulsion that weakens the pinning effect of the vortex traps; both effects tend to degrade the dc vortex response.

IV. VORTEX TRAJECTORIES FOR DIFFERENT AC DRIVE PERIODS

In Figs. 4(a)–4(d), we display the pinning sites (open circles), vortex positions (dots) and 2D vortex trajectories (lines) at $H/H_1 = 1.05$ for different half-periods P of the ac drive. Here, we set the drive amplitude to $F_L = 0.3$ and chose $d = 0.2a_0$, $F_{p0}^s/F_{p0}^w = 2$.

When the period of F_L is small, (e.g., $P \sim 600\tau_0$), the interstitial vortices can move back and forth in the driving direction and one can see clearly their trajectories in Fig. 4(a). The trapped vortices can move out of the pinning centers when $\mathbf{F}_L \parallel \mathbf{y}$ (namely, points from the strong to the weak pinning site in each unit), but the travelling distance is smaller than the spacing a_0 of the pinning lattice. As $\mathbf{F}_L$ reverses sign, these vortices will be driven back to their original pinning centers; no net vortex transport takes place.

In Fig. 4(b), at $P = 800\tau_0$, during the half period when a driving force with $F_L > F_m$ points in the y direction, the initially trapped vortices can move out of the pinning centers and travel a distance equal or larger than the lattice constant
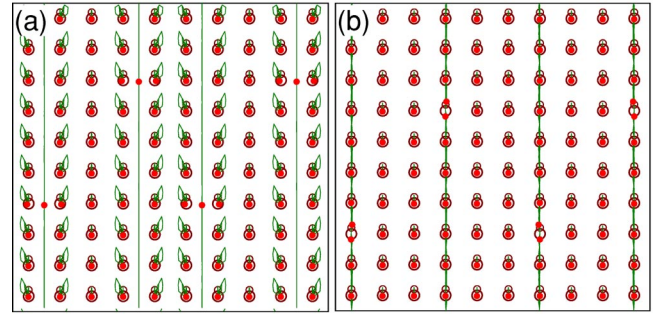
a_0. These vortices may get trapped again, but in a nearby pinning center. During the subsequent drive half-period, when $\mathbf{F}_L$ points in the negative y-direction (namely, from the weak to the strong pinning sites in each unit), the commensurate vortex rows cannot be driven back to their original pinning centers, because F_L is smaller than the stopping force F_M of the strong pinning sites. Thus, the system behaves as a "collective vortex step motor," *collectively shifting all pinned vortices by one step for each cycle*. In the asymmetric pinning arrays considered here, each pinning unit can only trap one vortex. So, the more efficient net vortex response to the ac driving force occurs at or below the first matching field, $H/H_1 \lesssim 1$, as shown in Fig. 2(b).

In Fig. 4(c), we display the 2D vortex trajectories for $P = 1000\tau_0$, i.e., around the mid-point of the first sawtooth of the corresponding $V_{dc}(P)$ curve in Fig. 2(a). We observe a stationary dynamical regime, in which the interstitial vortices move back and forth a distance larger than a_0, but with no net displacement in either direction, while the commensurate vortex rows advance a step a_0 per cycle in the positive y-direction.

Figure 4(d) shows the 2D vortex trajectories for $P = 1600\tau_0$, right after and very close to the tip of the second sawtooth in the relevant $V_{dc}(P)$ plot. Here, the interstitially flowing vortices disappear as they get absorbed in vertically moving columns of vortices, which now flow slower in the form of "soliton-like" discommensurations. This stationary vortex flow phase can be also found in the dc driven case[20] (see Sec. XI).

Finally, in Fig. 5 we focus on the interstitial dynamics in the subthreshold regime $F_L < F_m$, where no collective vortex motion takes place. For $F_L = 0.225$ the untrapped vortices can be found in two distinct dynamical phases, depending on the drive half-period: in panel (a) each interstitial runs parallel to $\mathbf{F}_L$ at the center of the channel delimited by the two adjacent (locked) vortex columns. Its average net velocity is *negative*; in panel (b) the moving vortices form mobile discommensurations. Discommensuration-bearing columns drift in the *positive* direction like the regular vortex columns when $F_L > F_m$. The interstitial response to the ac drive is respon-
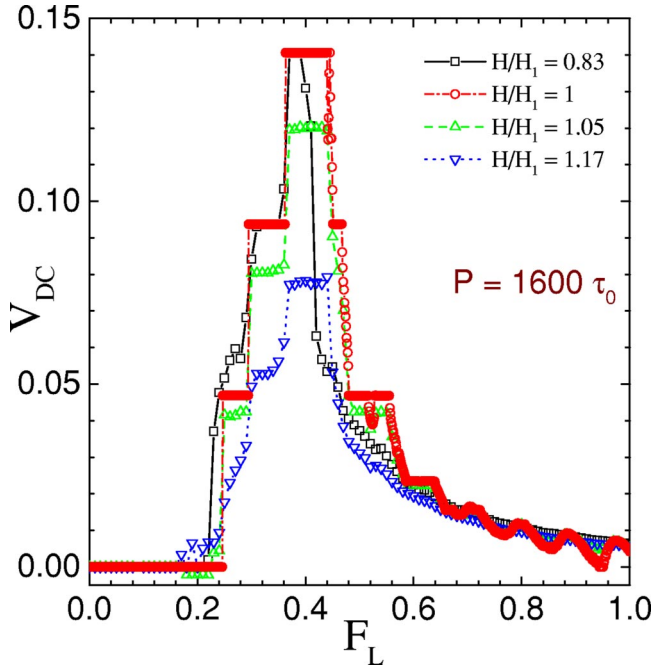

FIG. 5. (Color online) Vortex trajectories in the subthreshold regime $F_L = 0.225$ for $H/H_1 = 1.01$, and different drive half-periods: (a) $P = 1000\tau_0$, interstitial phase with negative average velocity; (b) $P = 1800\tau_0$, discommensuration phase with positive average velocity. The remaining simulation parameters are as in Fig. 4.

FIG. 6. (Color online) Dependence of the net average velocity V_{dc} on the drive amplitude F_L: squares, $H/H_1 = 0.83$; circles, $H/H_1 = 1$; upward triangles, $H/H_1 = 1.05$; downward triangles: $H/H_1 = 1.17$, with fixed half-period $P = 1600\tau_0$. Here, $d = 0.2a_0$, $F_{p0}^s/F_{p0}^w = 2$, $\tau_0 = 0.0067$, and $F_{T_0} = 0$.

sible for the small negative V_{DC} values reported in Figs. 2 and 6.

V. AMPLITUDE DEPENDENCE OF THE NET DC VOLTAGE

The plots in Fig. 6 clearly show that the ac driven vortex transport is appreciable only within the drive amplitude range (F_m, F_M); the peak of the $V_{dc}(F_L)$ curves is centered at an optimal rectification value F_L and decreases with the ratio of the vortex density to the pins in the sample. Both the plateaus of the dc response curves and the damped oscillations of their tail are consequences of the constant drive period used here. A larger amplitude F_L forces the vortices to cross more pinning sites in each positive drive half-period P, thus producing a new plateau for each additional pinning unit they cross. These turn into damped oscillations when the driving force F_L overcomes the stopping force F_M of the strong pinning sites [see Fig. 3(d) for a vortex trajectory at $F_L > F_M$].

For $H/H_1 = 1$, the $V_{dc}(F_L)$ curve exhibits neat, flat plateaus corresponding to commensurate lock-in transitions, where the amplitude of the back-and-forth motion of the vortices matches the distance a_0 between pinning sites (see Sec. XI). These lock-in plateaus are the analogs of the "Arnold's tongues" described in Ref. 21. The main lock-in plateaus are separated by sharp steps. When $H/H_1 > 1$, the presence of interstitial vortices blur the collective stepwise vortex motion in the positive direction (the stopping force F_m weakens, too) and the corresponding V_{dc} plateaus get smeared out to form the damped oscillations shown in Fig. 6.
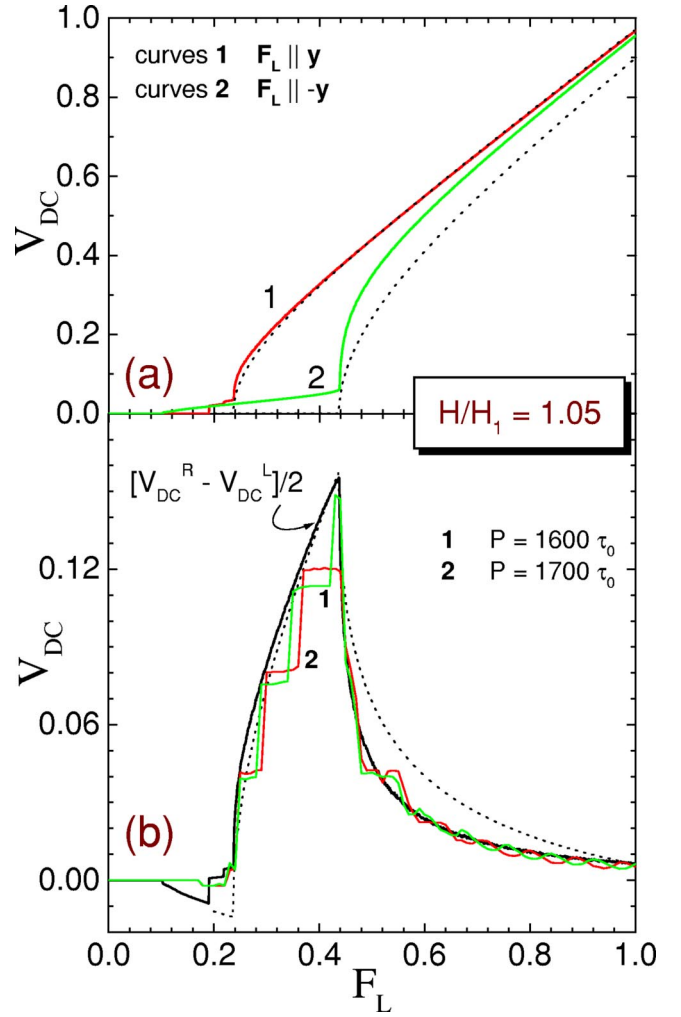

FIG. 7. (Color online) Average velocity V_{dc} vs F_L for (a) dc current drive along **y** (curve 1) and $-$**y** (curve 2), and (b) ac drive along **y** (thin curves) at $P = 1600, 1700\tau_0$, and half the difference between the two dc-driven curves in (a) (thick curve). Here, $H/H_1 = 1.05$, $d = 0.2a_0$, $F_{p0}^s/F_{p0}^w = 2$, $\tau_0 = 0.0067$, and $F_{T_0} = 0$. The one-particle analytical prediction in Eq. (10) for $u_{R,L}$ are plotted in (a) for comparison (dotted curves); the approximate adiabatic V_{dc}-F_L characteristic curve described in Sec. XI is drawn in (b) as a dotted curve.

VI. COMPARISON BETWEEN AC AND DC DRIVES

To better analyze the ratchet effect of asymmetric pinning systems, it is interesting to study the vortex response to dc drives in opposite y directions. In Fig. 7(a), we report the stationary average vortex velocities $V_{dc}^R(F_L)$ and $V_{dc}^L(F_L)$, versus the amplitude of a dc drive with $\mathbf{F_L}\|\mathbf{y}$ and $\mathbf{F_L}\|-\mathbf{y}$, respectively. The effect of the asymmetric pinning is apparent. Indeed, it is easier to depin vortices when driven in the positive direction ($\mathbf{F_L}\|\mathbf{y}$) since the weaker pins are easier to overcome. A more detailed study of the asymmetric pinning effect in the presence of a dc drive can be found in Ref. 15.

In Fig. 7(b), we compare the curve $[V_{dc}^R(F_L) - V_{dc}^L(F_L)]/2$, computed from the data in Fig. 7(a), with the net average response $V_{dc}(F_L)$ to an ac drive as a function of the amplitude F_L at fixed half-periods $P = 1600\tau_0$, and
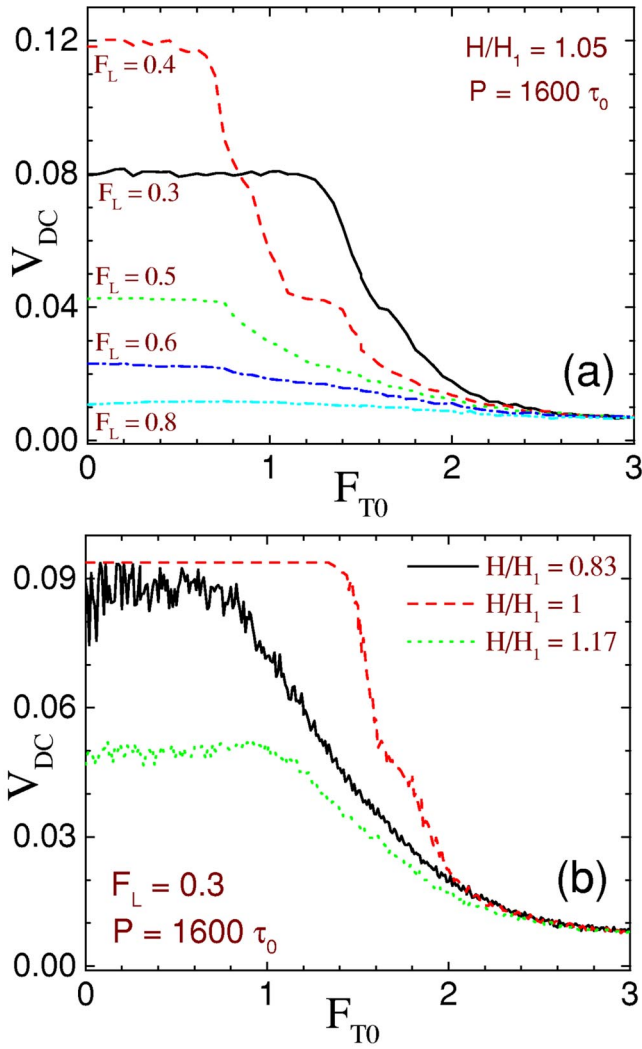
FIG. 8. (Color online) (a) Net average velocity V_{dc} vs the amplitude F_{T_0} of the thermal noise force F_T for the ac driven case for different amplitudes, $F_L = 0.3$, 0.4, 0.5, 0.6, and 0.8, and fixed magnetic field density, $H/H_1 = 1.05$. (b) Net average velocity V_{dc} for different ratios H/H_1 of vortices to pins in samples with $H/H_1 = 0.83$, 1, 1.17, and drive amplitude $F_L = 0.3$. Here, $d = 0.2a_0$, $F_{p0}^s/F_{p0}^w = 2$, $\tau_0 = 0.0067$, and $P = 1600\tau_0$.

$1700\tau_0$. Notice that in the case of a square-wave drive, $[V_{dc}^R - V_{dc}^L]/2$ can be regarded as an *adiabatic* approximation to the rectified voltage V_{dc}; this explains the close agreement between the two curves plotted in Fig. 7(b).

VII. EFFECT OF THERMAL FLUCTUATIONS

In Fig. 8, we show the effect of thermal noise on the dc response of the vortex motion. As seen in Fig. 8(a), when the thermal noise strength F_{T_0} is sufficiently small, V_{dc} is almost "locked" because the vortex lattice moves somewhat "rigidly" due to the vortex-vortex interaction. On increasing F_{T_0} above a certain value, which depends on F_L, the average dc velocities of the vortices drop rapidly. This is seen more clearly in the vicinity of F_M of the optimal value $F_L \sim 0.4$

[Fig. 8(a)] and for magnetic fields close to the first matching field [Fig. 8(b)].

When the applied magnetic fields are either larger or smaller than the first matching field $H/H_1 = 1$, thermal fluctuations in the vortex response are more pronounced, see Fig. 8(b). Therefore, the addition of thermal noise in the simulation *always* weakens vortex transport. This is quite different from other types of "rectifiers" (see, e.g., Refs. 1 and 22) where a broad peak in the net average velocity versus temperature was observed.

VIII. ASYMMETRY DEPENDENCE OF THE DC RESPONSE

A. Dependence on the pin-lattice mismatch

To investigate the effect of the asymmetry on the vortex motion, it is interesting to vary the parameters of the two square pinning sublattices. Here, we keep focusing on the incommensurate case $H/H_1 = 1.05$ with fixed drive half-period $P = 1600\tau_0$. In Fig. 9(a), we display V_{dc} as a function of the separation d between the weak and strong pinning sublattices; the pinning amplitudes F_{p0}^s and F_{p0}^w are the same as in the figures above.

When $d = 0$, i.e., the two pinning sublattices overlap, the pinning geometry is perfectly symmetric and, as expected, the vortex response V_{dc} vanishes. On increasing d, a nonzero dc response appears due to the asymmetry of the pinning traps. When the composite pinning centers reach an optimal asymmetry (for $d \sim 0.2a_0$), the $V_{dc}(d)$ curves hit their maximum value (this behavior is apparent for $F_L \sim F_M$). For a sufficiently large separation between the two pinning sublattices (e.g., $0.4a_0 \lesssim d \lesssim 0.5a_0$), the two sets of pinning sites no longer overlap; the effective pinning potential $U_p(y)$ turns symmetric again and the vortex dc response drops back to zero.

B. Dependence on the pinning amplitude ratio

Another method to characterize the asymmetry of the pinning potential is to vary the pinning amplitude ratio F_{p0}^w/F_{p0}^s of the two square pinning sublattices. In Fig. 9(b), we show V_{dc} for various amplitudes of the ac driving force as a function of the amplitude ratio F_{p0}^w/F_{p0}^s with fixed values $F_{p0}^s = 0.5$ and $d = 0.2a_0$. Here, we still focus on the incommensurate case $H/H_1 = 1.05$ at a fixed half-period $P = 1600\tau_0$.

When $F_{p0}^w/F_{p0}^s = 0$, i.e., the pinning strength of the weak pinning sublattice is $F_{p0}^w = 0$, the asymmetry of the ratchet pinning potential $U_p(y)$ disappears; as a result the dc response is null. On increasing F_{p0}^w/F_{p0}^s, the asymmetric pinning effect becomes detectable due to the partial overlap of the two pinning sublattices, until for an optimal asymmetry ratio $F_{p0}^w/F_{p0}^s \simeq 0.5$, the vortex dc response attains a maximum. As the strength of the weak pinning sites F_{p0}^w approaches F_{p0}^s, i.e., $F_{p0}^w/F_{p0}^s \simeq 1$, the asymmetry of the pinning potential vanishes again, and so does the net vortex transport in Fig. 9(b).

The rectifying power of a ratchet device can be quantified in terms of an asymmetry factor proportional to the differ-
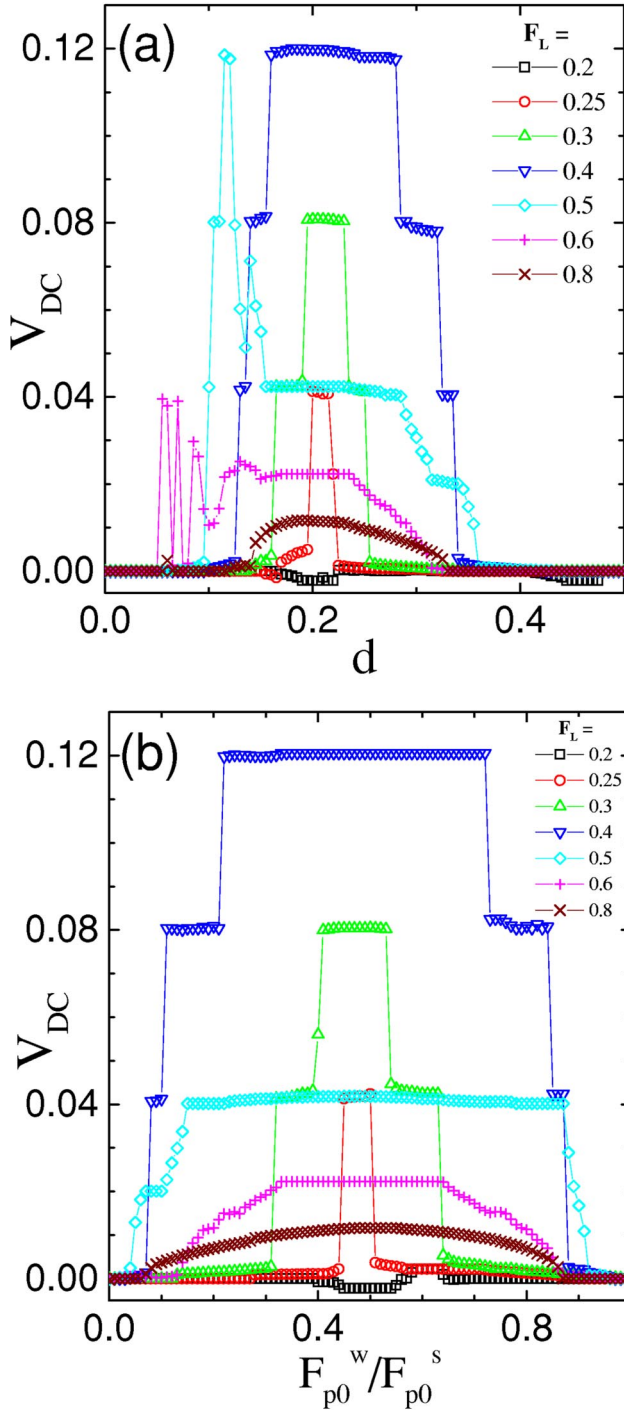
FIG. 9. (Color online) (a) Dependence of the net average velocity V_{dc} on the separation d between the strong and the weak pinning square sublattices. $F_{p0}^s/F_{p0}^w = 2$. (b) Dependence of the net average velocity V_{dc} on the ratio F_{p0}^s/F_{p0}^w between the amplitudes of the strong and the weak pinning sit with fixed $F_{p0}^s \equiv 0.5$ at $d = 0.2a_0$. In both figures, the half-period P of the ac driving force is $P = 1600\tau_0$, F_L varies from 0.2 to 0.8, $F_{T_0} = 0$, $\tau_0 = 0.0067$, and $H/H_1 = 1.05$.

ence between the stopping forces, $F_M - F_m$. The *asymmetry factor* is a crucial figure of merit or key parameter characterizing the performance of this type of devices. Figure 10
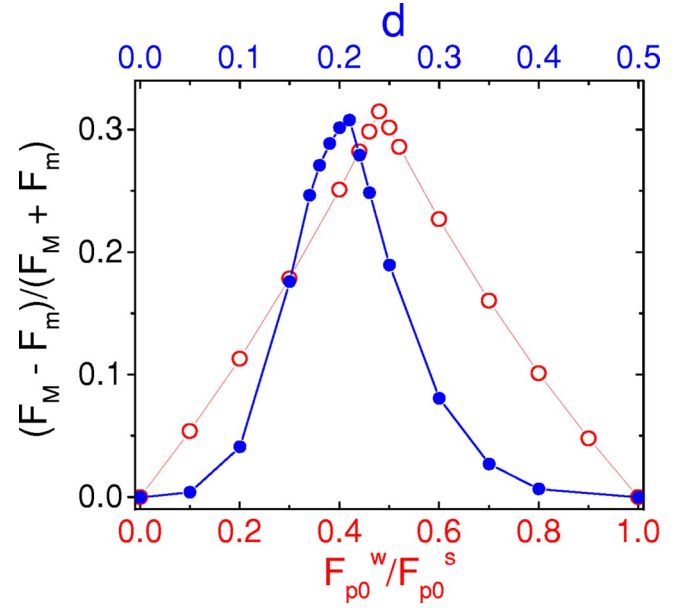

FIG. 10. (Color online) Asymmetry factor $(F_M - F_m)/(F_M + F_m)$ as a function of the ratio F_{p0}^w/F_{p0}^s (bottom axis) at $F_{p0}^s = 0.5$ and $d = 0.2a_0$ (open circles), and of the sublattice distance d (upper axis) for $F_{p0}^s/F_{p0}^w = 2$ (solid circles). The asymmetry factor represents the difference between the critical depinning forces, normalized to twice the average depinning force.

shows the ratio of the difference between the stopping forces, $F_M - F_m$, over twice their average $F_M + F_m$ as a function of both d and also F_{p0}^w/F_{p0}^s. This asymmetry factor is very clearly peaked at $d \approx 0.21$ and $F_{p0}^w/F_{p0}^s \approx 0.48$. Also notice that both curves are similar and that the $F_M - F_m$ dependence on the separation d between the strong and weak pinning centers is apparently consistent with the simulation results in Fig. 9(a), which indicated an optimal d near 0.2.

IX. EFFECTS OF PINNING DISORDER

In this section we study systematically the effects of both the translational and the angular disorder of the asymmetric pinning units. For an easier comparison with the results of the foregoing sections, we keep the following simulation parameters fixed: $H/H_1 = 1.05$, $P = 1600\tau_0$, $d = 0.2a_0$, $F_{p0}^s = 0.5$, and $F_{p0}^s/F_{p0}^w = 2$.

A. Spatial disorder

A controllable amount of disorder in the pinning lattice can be simulated by displacing each pinning center from its square lattice position $\mathbf{R}_{i0}$ at random[20,23] according to the rule

$$\mathbf{R}_i = \mathbf{R}_{i0} + a_0 \Delta R_{\text{disorder}} (\nu_x \mathbf{x} + \nu_y \mathbf{y}).$$

Here, $\mathbf{R}_i$ is the final location of the ith pinning unit, ν_x and ν_y are random numbers uniformly distributed between -1 and 1 and $\Delta R_{\text{disorder}}$ gauges the amount of disorder.

In Fig. 11(a), we show the dc vortex current as a function of the drive amplitude F_L for different values of $\Delta R_{\text{disorder}}$. On increasing the amount of spatial disorder, the peak value
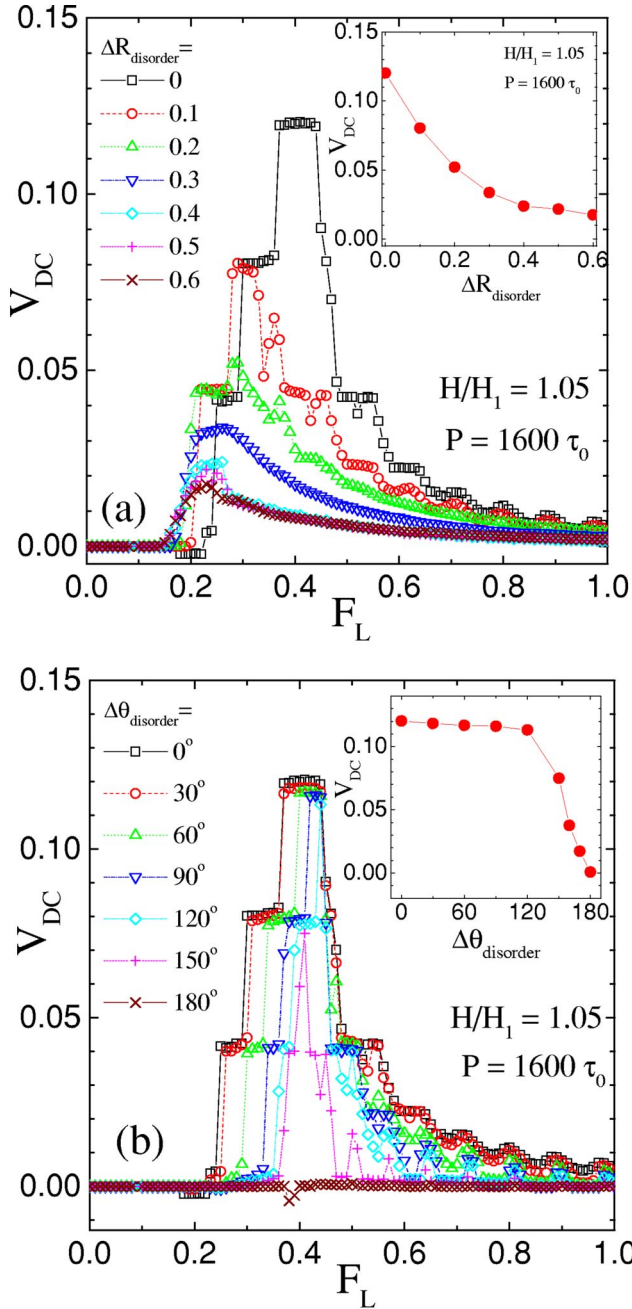
FIG. 11. (Color online) (a) Dependence of the net average dc velocity V_{dc} on the amplitude of the ac drive force for increasing values of the translational disorder parameter ($\Delta R_{disorder} = 0, 0.1, \ldots, 0.6$) of the pinning centers. The inset shows the dependence of the maximum values of V_{dc} in the curves $V_{dc}(F_L)$ on the disorder strength parameter $\Delta R_{disorder}$. (b) Dependence of the net average velocity V_{dc} on the amplitude of the ac drive for increasing values of the orientational disorder parameter ($\Delta \theta_{disorder} = 0, 30°, \ldots, 180°$) of the asymmetric pinning sites. The inset shows the dependence of the maximum values of V_{dc} in the curves $V_{dc}(F_L)$ on the disorder parameter $\Delta \theta_{disorder}$. In both figures, the half period P of the ac driving force is $P = 1600 \tau_0$, $d = 0.2 a_0$, $F_{p0}^s / F_{p0}^w = 2$, $F_{T_0} = 0$, $\tau_0 = 0.0067$, and $H/H_1 = 1.05$.

of the V_{dc}-F_L characteristics decreases, while its plateau structure disappears altogether at large $\Delta R_{disorder}$. The peak

value of $V_{dc}(F_L)$ as a function of $\Delta R_{disorder}$ is shown in the inset of Fig. 11(a). We emphasize that even if we scramble the *location* of the asymmetric pinning centers to an effectively random distribution, here their *orientation* is maintained parallel to $+\mathbf{y}$. This explains why in the inset of Fig. 11(a) the maximum vortex ratchet current approaches a finite asymptotic value ~ 0.2 for $\Delta R_{disorder} > 0.4$.

B. Angular disorder

The angular disorder of the asymmetric pinning sites can be simulated by displacing the weak pinning center around the strong one in each pinning unit, while keeping their separation $d = 0.2 a_0$ fixed. We define $\Delta \theta_{disorder}$ as the maximum deviation of the angle between the symmetry axis of the composite pinning unit (oriented from the strong to the weak pinning centers) and the positive y axis, i.e.,

$$\theta_i = \nu_\theta \Delta \theta_{disorder}.$$

Here, $\nu_\theta \in [-1,1]$ is a random number uniformly distributed and θ_i is the new (random) orientation of the ith pinning unit.

In Fig. 11(b), we show the vortex current as a function of the drive amplitude F_L for different values of $\Delta \theta_{disorder}$. With increasing the angular disorder $\Delta \theta_{disorder}$, the maximum of the V_{dc} is largely insensitive to $\Delta \theta_{disorder}$ as long as $\Delta \theta_{disorder} \lesssim 120°$. Moreover, as $\Delta \theta_{disorder}$ grows larger than $120°$, the peak value of the $V_{dc}(F_L)$ curves drops quickly; their plateaus shrink and eventually vanish. Finally, for $\Delta \theta_{disorder} = 180°$, i.e., when the angular disorder of the pinning lattice is complete, no rectification of the ac driven vortex motion is detectable.

C. Devil staircases and Arnold's tongues

Devil staircase structures with many plateaus of different sizes can appear in systems with two competing periodicities. In our samples, one periodicity is temporal (the applied ac drive, producing periodic spatial oscillations of vortices in a sample with no pins), while the other periodicity is spatial (the periodic array of pinning centers). Physical examples of ac driven systems exhibiting devil staircase structure include charge density waves and Josephson junctions. The plateaus are also known as phase-locking regions, and the widest plateaus are typically the ones near the center of the staircase structure, which is also the case in our system. The width of these plateaus can change as a function of the system parameters, forming distorted elongated triangles or "Arnold's tongues."

Our system here has many degrees of freedom, which interact with each other and also with the many potential wells in the sample. This is similar to another vortex system[21] and in contrast with the typical nonlinear circle maps (which exhibit very clean and mathematically well defined devil staircases and Arnold's tongues) that only have two degrees of freedom, as opposed to very many as in our case.

Figure 12 shows a diagram of the width of the plateaus of V_{dc} versus F_L for an increasing degree of orientational dis-
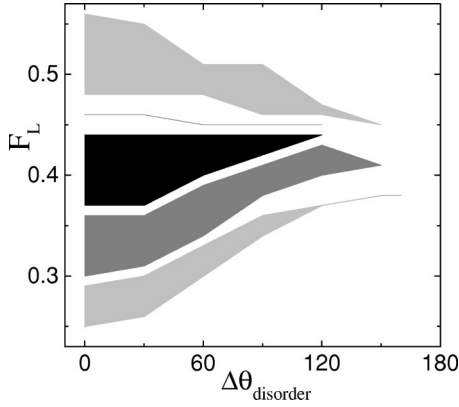
FIG. 12. Width of the plateaus in V_{dc} [shown in Fig. 9(b)] vs the degree of orientational disorder $\Delta\theta_{\text{disorder}}$ of the asymmetric pinning centers. These plateaus in V_{dc} follow a devil staircase with an Arnold's tongue structure (which is shaded in the figure). These shaded tongues correspond to $V_{dc} \approx 1.2$ (black), 0.8 (gray), and 0.4 (light gray), in Fig. 11(b) for various values of $\Delta\theta_{\text{disorder}}$. The remaining simulation parameters are $P = 1600\tau_0$, $d = 0.2a_0$, $F_{p0}^s/F_{p0}^w = 2$, $F_{T_0} = 0$, $\tau_0 = 0.0067$, and $H/H_1 = 1.05$.

order $\Delta\theta_{\text{disorder}}$. When the latter is zero, the width of the plateaus is maximum. When it increases to $30°, 60°, 90°$, and so on, two general trends can be observed: (a) the width of the V_{dc} plateaus shrinks, and (b) these tend to shift to higher values of F_L.

These results are physically reasonable and can be explained as follows: Increasing the degree of orientational disorder decreases the effectiveness of the rectifier by missaligning the pin units with respect to each other (thus, shrinking the width of the V_{DC} plateaus) and requires slightly higher values of F_L to achieve similar levels of rectification (thus shifting the plateaus to higher values of F_L). The shrinking plateaus shown in Fig. 12 are known as Arnold's tongues in the literature on commensurate-incommensurate systems.

X. SAMPLE SIZE DEPENDENCE

To further confirm our simulation results and conclusions, we have tested our simulations for various sample sizes. In Fig. 13, we show results of our simulations in 10×10, 10×16, 20×16, 20×20, and 30×30 pinning lattice systems at fixed magnetic field density $H/H_1 = 1.05$. The spacing between pinning sites is always a_0. Notice that the actual number of vortices grows with the number of pinning sites. The other parameters are chosen as $d = 0.2a_0$, $F_{p0}^s/F_{p0}^w = 2$, $F_L = 0.3$ and $F_{T_0} = 0$. The original vortex lattices for each case are obtained from similar annealing processes.

As seen in Fig. 13, the onset, the oscillation period and the strength of the dc response V_{dc} for the vortex motion versus the half period P of the ac drive are essentially the same for all these systems. The unavoidable minor fluctuations are due to the disorder of the vortex lattice at the incommensurate magnetic field density $H/H_1 = 1.05$. Some additional very small peaks (the most visible ones near $P = 2000\tau_0$ and $P = 2500\tau_0$ for $N_p = 400$ pinning sites) are due
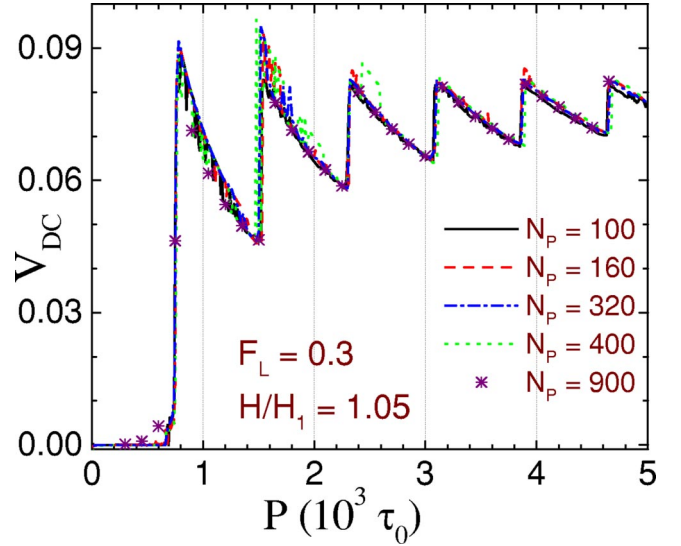

FIG. 13. (Color online) Net average vortex dc velocity V_{dc} vs the half-period P of the ac driving force for different sizes of the simulation system: $N_p = 100$, 160, 320, 400, 900 for a *fixed* magnetic field density $H/H_1 = 1.05$. Even though the system size grows, the number of vortices is always 5% higher than the number of pinning sites. Here, $F_L = 0.3$, $d = 0.2a_0$, $F_{p0}^s/F_{p0}^w = 2$, $F_{T_0} = 0$, and $P = 1600\tau_0$.

to the fact that sometimes interstitial vortices, that normally drift in the negative direction, are either dragged along by the moving vortex lattice (Stokes' drift[24]) or join altogether a moving vortex column thus becoming a *discommensuration* (see Fig. 5). Discommensuration-bearing columns advance in the positive direction, which translates into higher values of $V_{dc}(P)$, as seen in Fig. 13.

XI. ANALYTICAL DISCUSSION

A full analytical interpretation of the vortex ratchet flows simulated above lies beyond the reach of today's non-equilibrium statistical mechanics. Nevertheless, close to the first matching field $H/H_1 = 1$ there are no interstitial vortices and therefore the overall vortex dynamics can be analyzed to a good accuracy through a simplified one-particle approach. The current literature on overdamped ratchets in one dimension can thus provide us with the necessary guidance.[22,25–32]

For $H/H_1 = 1$ the effects of the vortex-vortex interaction cancel out for geometrical reasons so that we can just ignore them. The net potential $U_p(y)$ felt by a noninteracting vortex moving parallel to the applied Lorentz force in the **y** direction, results from the linear superposition of all pinner potentials, corresponding to pinning forces (1), along one lattice column. As one can see from Fig. 1(a), $U_p(y)$ is a periodic asymmetric potential capable of sustaining a ratchet current[22,25,26]; in the absence of thermal fluctuations its rectifying power is mostly limited to the amplitude window (F_m, F_M), with $F_m < F_M$. We recall that the two limiting values F_m and F_M can be computed numerically from Eq. (1): For the pinning parameters shown in Fig. 1, $F_m \simeq 0.236(\sim 0.25 = F_{p0}^w)$ and $F_M \simeq 0.436(\sim 0.5 = F_{p0}^s)$ [also see Fig. 7(a)]. Indeed, as discussed before, it is physically

reasonable to expect that $F_m \sim F_{p0}^w$ and $F_M \sim F_{p0}^s$.

The curve V_{dc} versus P for $H/H_1 = 1$ in Fig. 2(b) can be reproduced fairly closely. First of all, we need to determine the activation half period P_c, when the rectification mechanism sets on all of a sudden: P_c must be long enough for a single vortex to drift from one pinning well to the adjacent one along a **y** column, by climbing the less steep side of the $U_p(y)$ well it sits in [i.e., in the positive **y** direction for the $U_p(y)$ potential of Fig. 1]. The net vortex velocity $\langle u \rangle$ over such a distance is a nonlinear function of F_L. A rough estimate of $\langle u \rangle$ can be given by assuming that the vortex velocity inside a pinning well tilted in the positive direction with $F_L > F_m$ is $F_L - F_m$, while in the flat region between pinners is just F_L (remember that the viscous constant η has been set to one). In other words, $\langle v \rangle \sim F_L - F_m$ [when $F_L > F_m$ and $\langle v \rangle \sim F_L$ in the space between traps]. Also, the longitudinal size of the double pinning well structure in Fig. 1 can be conveniently approximated to $\delta_p = 2R_p + d$ ($=0.46a_0$ here). Thus,

$$\langle u(F_L) \rangle = \kappa(F_L)F_L = F_L \left(1 - \frac{\delta_p F_m}{F_L} \right). \qquad (5)$$

For the sake of a comparison with the simulation data reported in Figs. 2–8 the explicit value of the correcting factor is $\kappa(F_L = 0.3) \simeq 0.64$. Our estimate for the half period P_c is then

$$P_c = \frac{a_0}{\langle u \rangle} = \frac{a_0}{\kappa(F_L)F_L}. \qquad (6)$$

In Fig. 2(b), $a_0 = 150\tau_0$, and therefore prediction (6) for P_c yields $P_c = 780\tau_0$ within less than 2% from the numerical estimate $760\tau_0$ from our simulation.

The curve V_{dc} vs P in Fig. 2(b) shows a sequence of peaks of the same height $V_{dc} = V_M$. These peaks appear at the following periods:

$$P(\text{maximum } V_{dc}) = nP_c + \varepsilon,$$

where ε is very small, i.e., to the driving condition when a single vortex can advance by exactly n lattice constants a_0 in the **y** direction during half a forcing cycle (getting immediately trapped as $\mathbf{F_L}$ reverses its sign). The peak velocity is therefore

$$V_M = \frac{na_0}{2nP_c} = \frac{\kappa(F_L)F_L}{2}. \qquad (7)$$

The minima $V_m(n)$ of the curve V_{dc} versus P at $H/H_1 = 1$ occur at these periods:

$$P(\text{minimum } V_{dc}) = nP_c - \varepsilon,$$

as the vortex drifts a distance na_0 in a half-period of duration $(n+1)P_c$; accordingly,

$$V_m(n) = V_M \frac{n}{n+1}, \qquad n = 1, 2, 3, \ldots . \qquad (8)$$

Both predictions for V_M and $V_m(n)$ are displayed in Fig. 2(b) as compelling evidence of the one-particle approach when $H/H_1 \sim 1$.

Figure 6 shows a typical plot of the ratchet current V_{dc} versus the drive amplitude F_L: For $P = 1600\tau_0$ the first three horizontal steps of the V_{dc} versus F_L characteristics have roughly similar widths $\Delta F_L \simeq 0.07$ and are equally spaced with $\Delta V_{dc} \simeq 0.047$. Both features are well reproduced by the heuristic argument in Eqs. (5) for the average net vortex velocity $\langle u(F_L) \rangle$ and Eq. (6) for the period P_c. Periodic jumps in the $V_{dc}(F_L)$ curve occur for the discrete solutions $F_L = F_n$ of the equation

$$F\kappa(F)P_c = na_0,$$

namely

$$F_n = nF_0 + \delta_p F_m, \qquad (9)$$

with $F_0 = a_0/P_c$. When $P_c = 1600\tau_0$, then $F_0 = a_0/P_c = 0.0938$. Only two jump amplitudes F_n fall within the rectification window (F_m, F_M), i.e., $F_2 \simeq 0.30$ and $F_3 \simeq 0.36$ ($F_1 \approx 0.2$ is shifted to 0.24, because V_{dc} is zero below $F_m \sim 0.24$). As a consequence, the rising branch of the V_{dc} versus F_L characteristics plot exhibits only three horizontal steps

$$V_{dc}(n) = n\Delta V_{dc},$$

with $n = 1, 2, 3$ and $\Delta V_{dc} = a_0/P_c = 0.047$. For $P/\tau_0 = 3200$ (4800) the simulation reveals six (nine) jumps within the rectification window (not shown here) in agreement with Eq. (9). The favorable comparison thus achieved establishes the validity approximation (5) over the entire rectification window (possibly with appreciable deviations in the vicinity of F_m).

Finally, Fig. 7 also deserves a closer inspection. The upper panel shows the stationary velocities

$$V_{dc}^R = V_{dc}(+F_L)$$

and

$$V_{dc}^L = V_{dc}(-F_L)$$

of a single vortex driven to opposite directions by a dc signal of intensity F_L, in the absence of thermal fluctuations $F_{T_0} = 0$ and for H slightly larger than its first matching value H_1 ($H/H_1 = 1.05$). On ignoring the role of the unpinned vortices (here fewer than 5%), we can try to extend the one-particle approach to this problem, as well. The velocity versus force u-F_L characteristics for a particle moving on a noiseless one-dimensional periodic substrate is reasonably well approximated by the formula

$$u_{R,L}(F_L) = \sqrt{F_L^2 - F_{m,M}^2} \qquad (F_L > F_{m,M}), \qquad (10)$$

which is exact in the case of a *sinusoidal* potential $U_p(y)$.[32] Here, one uses F_m if the vortex is being driven against the stopping force F_m (i.e., to the right), and vice versa.

In Fig. 7(a) the agreement between V_{dc}^R and u_R is by far much closer than between V_{dc}^L and u_L. The reason for this

discrepancy is twofold: (i) The right hand side of the potential wells in Fig. 1 are too steep to be fitted to a sinusoidal function with appropriate amplitude and wavelength. Apparently such an approximation works better for the lower slopes encountered by a vortex being pulled in the opposite direction. (ii) Interstitial tails are easily detected in both curves V_{dc}^R and V_{dc}^L, with the interstitial effect looking more pronounced in the negative direction, i.e. for V_{dc}^L.[15]

In Fig. 7(b) we compare the net velocity V_{dc} of the vortices subjected to a square-wave periodic signal $F_L(t)$ with the most obvious *adiabatic* approximation $[V_{dc}^R - V_{dc}^L]/2$. As shown by Bartussek *et al.*,[26] the adiabatic curve (for $P \rightarrow \infty$) embeds all the V_{dc} curves for finite P. Formulas (10) can be used to reproduce the adiabatic curve from simulation provided that one first adds an adequate interstitial tail to $u_L(F_L)$. For simplicity we fitted the interstitial tail of V_{dc}^L by means of a straight curve

$$u_L^i(F_L) = (H/H_1 - 1)F_L \quad \text{for} \quad 0 \leqslant F_L \leqslant F_M$$

and the constant offset

$$u_L^i(F_M) \simeq 0.022 \quad \text{for} \quad F_L > F_M;$$

the resulting adiabatic curve $[u_R(F_L) - u_L(F_L) - u_L^i(F_L)]/2$ is plotted in Fig. 7(b) for the sake of comparison. [We have implicitly assumed that the interstitial contribution to V_{dc}^L becomes negligibly small as F_L grows larger than F_M; the interstitial contribution to V_{DC}^R has been discarded altogether for simplicity.][34]

Both adiabatic V_{dc} curves suggest the existence of a small *negative* current peak due to the interstitial vortices, that at low forcing amplitudes (from the simulation $0.11 < F_L < 0.19$) appear to drift in the $(-\mathbf{y})$ direction. This reverse current is due to the interaction of the interstitial vortices with the pinned vortices. Note that the profile of the negative peak in the simulated adiabatic V_{dc} curve resembles the larger positive one. Indeed, we observed that in this forcing regime all interstitial vortices are confined between pairs of locked vortex columns subject to an effective potential with lower stopping forces, but with a reversed asymmetry with respect to $U_p(y)$. When the bound vortices spend more time in the deeper wells, the asymmetry of the vortex-interaction-based "interstitial pinning" is *reversed*, since the interstitial vortices are "repelled" from the deeper (occupied) wells. A detailed analysis of the interstitial dynamics lies outside the scope of the present work, and is described in a separate publication.[35]

XII. COMPARISON WITH OTHER VORTEX RECTIFIERS

The proposals in Refs. 1 and 3 are significantly different from the one here. A few differences, among others, include the following: (1) In Ref. 3 all pinned vortices do not move, while here they do. (2) In Ref. 3 only the motion of interstitial vortices is rectified, while here only the motion of interstitial vortices is not rectified (besides a very small interstitial effect which appears only for subthreshold drives, $F_L \leqslant F_m$). (3) In Ref. 3 all individual pins are symmetric, while here these are nonsymmetric. (4) In Ref. 3 the coarse-grained (spatial scale of $\sim \lambda$) pinning landscape is nonsymmetric, while here it is symmetric. (5) In Ref. 3 there is no "current inversion" when varying the applied force, while here there is. (6) Very importantly, in Ref. 3 there is no controllable "stepmotor" of vortices, while here there is. Thus, the systems in Ref. 3 and the one proposed here are significantly different, often opposite.

Furthermore, the system in Ref. 1 is vastly different from the one in Ref. 3 and the one described in this manuscript. For instance, items (1) to (6) above are not directly applicable to Ref. 1 because: Ref. 1 has (a) no interstitial vortices, (b) it has no individual pins acting directly on the moving vortices, (c) it has no current inversion, (d) it shows no controllable step-motor behavior, (e) its performance is optimal at intermediate temperatures instead of at low temperatures for Ref. 3, etc. The device in Ref. 1 is a completely different type of system from others, possibly the first boundary-type ratchet ever proposed. From the point of view of microfabrication, the proposal in the manuscript could be easily implemented via lithography, while Ref. 3 has been realized at Argonne[4] via irradiation (although it could also be realized, using lithography).

Last but not least, in this work we derive analytically all the main features observed numerically, while Refs. 1 and 3 include no analytical work. In addition, other ratchet systems, e.g., Josephson junction arrays,[11,12] have very smooth potentials, limiting their rectifying power.

XIII. APPLICATION TO OTHER SYSTEMS, INCLUDING COLLOIDAL PARTICLES

It is important to emphasize that our results apply mutatis mutandis to arrays of Josephson junctions, colloidal systems, Wigner crystals, and any system with repelling moveable objects that can be pinned by a lattice of traps. For instance, it directly applies to colloidal particles flowing through a Pachinko-like array of laser beams. Our results here could form the basis of a technology to sort colloids or biological molecules.[36] The "dictionary" here is (i) magnetic $\rightarrow$ electrical interactions; (ii) vortices $\rightarrow$ micron-size colloidal particles; (iii) superconductor medium $\rightarrow$ liquid; and (iv) array of traps made by electron beam lithography $\rightarrow$ array of traps made by optical holography. Indeed, our proposal here can be easily implemented as in Ref. 37. This requires: (a) using holographic optical tweezers to create *two* interpenetrating arrays of "locally asymmetric pinning traps," with weak and strong wells within each trap, instead of one; and (b) applying an ac drive to colloidal particles (instead of a dc drive, as in Ref. 37). This would produce a very controllable way to collectively and orderly move particles forward by quantized distances. Thus, our proposal here could be easily made in the lab, and its dynamics readily visualized, as in Ref. 37. In addition, if some particles have different sizes, their dynamics would be different from the other particles, and this could be used for important applications (e.g., particle segregation and sorting at the microscale).[36] Evidence of this appears in recent experiments[37] motivated by simulations.[21] Thus, the impact of the proposal here goes beyond superconductors.

XIV. CONCLUSION

In summary, we have studied both numerically and analytically the transport of vortices in superconductors with regular arrays of asymmetric pinning centers when applying a time-dependent alternating "square wave" electrical current. The asymmetric pinning centers are modeled by the superposition of two interpenetrating square lattices of weak and strong pinning centers with separation d. We have found that the arrays of asymmetric pinning centers can induce a "diode effect" (Ref. 33) for the vortex motion which results in a nontrivial dc response when applying an ac current. We have found a striking oscillation of the V_{dc} response of the vortex motion versus the period of the ac drive. The optimum magnetic field density $H/H_1 = 1$ and the dependence of the V_{dc} response of the vortex motion on the amplitude F_L of the ac drive and on other parameters was studied. Moreover, the V_{dc} versus d phase diagram reveals a strong dependence of the nonzero dc response with ac driving for the vortices on the separation d between the two pinning sublattices in the present work. Finally, we have demonstrated that the calcu-lation results and our conclusions are not dependent on the size of the simulation systems used in our study. The effects of disorder on the rectification are also obtained, showing a high degree of robustness against moderate amounts of disorder for the pinning traps. These show a clear devil Staircase type structure with plateaus in V_{dc} that behave like the Arnold tongues in dynamical systems and commensurate structures like charge density waves.

*Permanent address. Email address: nori@umich.edu

[1] J.F. Wambaugh, C. Reichhardt, C.J. Olson, F. Marchesoni, and F. Nori, Phys. Rev. Lett. **83**, 5106 (1999).

[2] C.S. Lee, B. Janko, I. Derenyi, and A.-L. Barabasi, Nature (London) **400**, 337 (1999).

[3] C.J. Olson, C. Reichhardt, B. Janko, and F. Nori, Phys. Rev. Lett. **87**, 177002 (2001).

[4] W.K. Kwok, R.J. Olsson, G. Karapetrov, U. Welp, V. Vlasko-Vlasov, K. Kadowaki, and G.W. Crabtree, Physica C **382**, 137 (2002).

[5] B.Y. Zhu, F. Marchesoni, V. V. Moshchalkov, and F. Nori (unpublished).

[6] S.E. Savel'ev and F. Nori, Nat. Mater. **1**, 179 (2002).

[7] *Applications of Superconductivity*, edited by H. Weinstock (Kluwer, Dordrecht, 1999); *SQUID Sensors*, edited by H. Weinstock (Kluwer, Dordrecht, 1996); *New Superconducting Electronics*, edited by H. Weinstock (Kluwer, Dordrecht, 1993); H. Weinstock, Physica C **209**, 269 (1993); IEEE Trans. Magn. **27**, 3231 (1991).

[8] I. Zapata, R. Bartussek, F. Sols, and P. Hänggi, Phys. Rev. Lett. **77**, 2292 (1996); I. Zapata, J. Luczka, F. Sols, and P. Hänggi, *ibid.* **80**, 829 (1998).

[9] S. Weiss, D. Koelle, J. Müller, R. Gross, and K. Barthel, Europhys. Lett. **51**, 499 (2000).

[10] E. Goldobin, A. Sterck, and D. Koelle, Phys. Rev. E **63**, 031111 (2001).

[11] E. Trías, J.J. Mazo, F. Falo, and T.P. Orlando, Phys. Rev. E **61**, 2257 (2000); J.E. Mooij, *et al.* (unpublished).

[12] F. Falo, P.J. Martinez, J.J. Mazo, and S. Cilla, Europhys. Lett. **45**, 700 (1999).

[13] G. Carapella and G. Costabile, Phys. Rev. Lett. **87**, 077002 (2001); G. Carapella, Phys. Rev. B **63**, 054515 (2001).

[14] D.J. Morgan and J.B. Ketterson, Phys. Rev. Lett. **80**, 3614 (1998).

[15] B.Y. Zhu, L. Van Look, V.V. Moshchalkov, B.R. Zhao, and Z.X. Zhao, Phys. Rev. B **64**, 012504 (2001).

[16] E.H. Brandt, J. Low Temp. Phys. **53**, 41 (1983).

[17] L. Van Look, B.Y. Zhu, R. Jonckheere, B.R. Zhao, Z.X. Zhao, and V.V. Moshchalkov, Phys. Rev. B **66**, 214511 (2002).

[18] F. Nori, Science **278**, 1373 (1996); C. Reichhardt, C.J. Olson, J. Groth, S. Field, and F. Nori, Phys. Rev. B **52**, 10 441 (1995); **53**, R8898 (1996); **54**, 16 108 (1996); C. Reichhardt, C.J. Olson, and F. Nori, *ibid.* **56**, 14 196 (1997); **57**, 7937 (1998); C.J. Olson, C. Reichhardt, and F. Nori, *ibid.* **56**, 6175 (1997); Phys. Rev. Lett. **80**, 2197 (1998); **81**, 3757 (1998).

[19] A. Brass and H.J. Jensen, Phys. Rev. B **39**, 9587 (1989); H.J. Jensen, A. Brass, A.C. Shi, and A.J. Berlinski, *ibid.* **41**, 6394 (1990); B.Y. Zhu, D.Y. Xing, J. Dong, and B.R. Zhao, Physica C **311**, 140 (1999).

[20] C. Reichhardt, C.J. Olson, and F. Nori, Phys. Rev. Lett. **78**, 2648 (1997); Phys. Rev. B **58**, 6534 (1998).

[21] C. Reichhardt and F. Nori, Phys. Rev. Lett. **82**, 414 (1999).

[22] P. Reimann, Phys. Rep. **361**, 57 (2002).

[23] B.Y. Zhu, J. Dong, and D.Y. Xing, Phys. Rev. B **57**, 5063 (1998).

[24] F. Marchesoni and M. Borromeo Phys. Rev. B **65**, 184101 (2002); Phys. Lett. A **249**, 199 (1998).

[25] C.R. Doering, W. Horsthemke, and J. Riordan, Phys. Rev. Lett. **72**, 2984 (1994).

[26] R. Bartussek, P. Hänggi, and J.G. Kissner, Europhys. Lett. **28**, 459 (1994); F. Marchesoni, Phys. Rev. E **56**, 2492 (1997); Phys. Lett. A **237**, 123 (1998).

[27] F. Jülicher, A. Ajdari, and J. Prost, Rev. Mod. Phys. **69**, 1269 (1997); R.D. Astumian, Science **276**, 917 (1997).

[28] F. Marchesoni, Phys. Rev. Lett. **77**, 2364 (1996).

[29] M. Borromeo, G. Costantini, and F. Marchesoni, Phys. Rev. E **65**, 041110 (2002).

[30] J. Rousselet, L. Salome, A. Ajdari, and J. Prost, Nature (London) **370**, 446 (1994); C. Keller, F. Marquardt, and C. Bruder, Phys. Rev. E **65**, 041927 (2002).

[31] I. Derényi and T. Vicsek, Phys. Rev. Lett. **75**, 374 (1995); I. Derényi and A. Ajdari, Phys. Rev. E **54**, R5 (1996).

[32] G. Costantini and F. Marchesoni, Europhys. Lett. **48**, 491 (1999).

[33] A flux-gradient-driven vortex diode using twin boundaries is de-

scribed in J. Groth, C. Reichhardt, C. J. Olson, S. Field, and F. Nori, Phys. Rev. Lett. **77**, 3625 (1996).

[34] Color versions of the figures in this work, and color videos of the vortex trajectories, can be found at http://www-personal.engin.umich.edu/~nori/stepmotor/.

[35] F. Marchesoni, B.Y. Zhu, and F. Nori, Physica A **325**, 78 (2003).

[36] C. Keller, F. Marquardt, and C. Bruder, Phys. Rev. E **65**, 041927 (2002).

[37] P.T. Korda, M.B. Taylor, and D.G. Grier, Phys. Rev. Lett. **89**, 128301 (2002); featured in Phys. Rev. Focus **10**, 12 (2002).